

A Study of Hadron Deformation in Lattice QCD

Constantia Alexandrou and Giannis Koutsou

Department of Physics, University of Cyprus, CY-1678, Cyprus

(Dated: November 6, 2018)

We develop the formalism for the evaluation of density-density correlators in lattice QCD that includes techniques for the computation of the all-to-all propagators involved. A novel technique in this context is the implementation of the one-end trick in the meson sector. Density-density correlators provide a gauge invariant definition for the hadron wave function and yield information on hadron deformation. We evaluate density-density correlators using two degenerate flavors of dynamical Wilson fermions for the pion, the rho-meson, the nucleon and the Δ . Using the one-end trick we obtain results that clearly show deformation of the rho-meson.

I. INTRODUCTION

Deformation in nuclei [1, 2] and atoms [3, 4] is an important phenomenon that has been extensively studied. In this work we address the question of whether deformation also arises in low-lying hadrons using the fundamental theory of the strong interactions, Quantum Chromodynamics defined on the lattice. In order to be able to answer this question we develop techniques for the exact evaluation of four-point correlators. These methods are also needed in a range of other applications in lattice QCD.

In this work we study the shape of the pion, the rho-meson, the nucleon (N) and the Δ . The pion being a spin-0 particle is expected to have no deformation and it therefore provides a check for our methodology. For particles with spin larger than 1/2, the one-body quadrupole operator provides a convenient characterization of deformation. The spin 1/2 nucleon cannot have a spectroscopic quadrupole moment but can still have an intrinsic deformation. The experiment of choice to reveal the presence of deformation in the nucleon and its excited state the Δ is measuring the N to Δ transition amplitude. Significant effort has been devoted to photo- and electro-production experiments on the nucleon at major experimental facilities [5, 6, 7, 8]. These experiments measure to high accuracy the ratios of the electric (E2) and Coulomb (C2) quadrupole amplitudes to the magnetic dipole (M1) amplitude. If both the nucleon and the Δ are spherical, then E2 and C2 are expected to be zero. There is mounting experimental evidence over a range of momentum transfers that E2 and C2 are non-zero [9, 10]. These ratios have been recently shown to be non-zero in lattice QCD [11] pointing to deformation in the nucleon or/and Δ .

A different approach that sheds light on deformation is to use density-density correlators to directly probe the hadron wave function [12, 13]. Density-density correlators [14, 15, 16, 17, 18, 19, 20, 21, 22, 23, 24] provide a gauge invariant definition of the hadron wave function. In a previous study [16] the density-density correlators were evaluated approximately. This was due to the fact that the all-to-all propagators needed for their exact evaluation were not calculated. Furthermore they

were computed for pion masses larger than 600 MeV and on lattices with a spatial volume of about 1.5 fm.

In this work we provide an exact evaluation of the four-point functions involved in the computation of the density-density correlators. The all-to-all propagators needed for the exact evaluation are calculated using stochastic techniques combined with dilution. In addition, we apply in the meson-sector for the first time in this context, the so-called one-end trick originally devised to evaluate the pion zero momentum two-point function [25]. In the two-point function, the one-end trick amounts to a clever summation of the spatial coordinates not only of the sink as routinely done but also of the source and therefore all-to-all propagators are involved. Implementation of this trick in the evaluation of the meson density-density correlators leads to a significant reduction of the statistical errors [24]. This trick, in its present formulation, can only be applied to meson density-density correlators. In baryons, the density insertions are on only two of the three quarks which gives rise to an odd number of quark propagators that cannot be grouped in pairs for the summation to work.

An alternative method applicable to both mesons and baryons is to combine stochastic evaluation of one all-to-all propagator with a sequential inversion to sum over the other spatial coordinate. This method, apart from the requirement of fixing the final hadronic state, needing new sequential inversions for each of the nucleon and Δ states, has been shown to yield results with similar errors as using two sets of stochastic inversions [22] We therefore do not consider it here.

Further improvements as compared to the previous study of density-density correlators [16] is that we use a spatial lattice of 24^3 as compared to 16^3 used previously and dynamical Wilson fermions corresponding to smaller pion masses, the lowest being 380 MeV.

This paper is organized as follows: In Section II we define the density-density correlators, in Section III we explain the stochastic techniques used for the evaluation of the all-to-all propagators, in Section IV we give the interpolating fields and parameters of the simulations and in Section V we describe our results on the density-density correlators for the pion, the rho-meson, the nucleon and the Δ and show how to correct for finite spatial volume effects. Finally in Section VI we summarize and give our

conclusions.

II. DENSITY - DENSITY CORRELATORS

Throughout this work we consider the equal-time density-density correlators defined by:

$$\begin{aligned}\tilde{C}_H(\vec{x}_2, t_1) &= \int d^3x_1 \langle H | j_0^u(\vec{x}_2 + \vec{x}_1, t_1) j_0^d(\vec{x}_1, t_1) | H \rangle \\ &= \int d^3x_1 \int d^3x \langle \Omega | J_H(\vec{x}, t) j_0^u(\vec{x}_2 + \vec{x}_1, t_1) j_0^d(\vec{x}_1, t_1) J_H^\dagger(\vec{x}_0, t_0) | \Omega \rangle\end{aligned}\quad (1)$$

where j_0^q is the normal ordered density operator : $\bar{q}\gamma_0q$: and J_H is an interpolating field with the quantum numbers of the lowest lying hadron H . The two integrals in Eq. (1) ensure that the state is projected to zero momentum; one integral sets the momentum of the sink equal to that of the source while the other sets both to zero. This can be shown explicitly by inserting three complete sets of states in Eq. (1):

$$\tilde{C}_H(\vec{x}_2, t_1) = \sum_{\vec{p}, n, n_i, n_f} \langle \Omega | J_H | n_f, \vec{0} \rangle \frac{e^{-E_{n_f}(\vec{0})(t-t_1)}}{2E_{n_f}(\vec{0})} \langle n_f, \vec{0} | j_0^u | n, \vec{p} \rangle \frac{e^{i\vec{p}\cdot\vec{x}_2}}{2E_n(\vec{p})} \langle n, \vec{p} | j_0^d | n_i, \vec{0} \rangle \frac{e^{-E_{n_i}(\vec{0})(t_1-t_0)}}{2E_{n_i}(\vec{0})} \langle n_i, \vec{0} | J_H^\dagger | \Omega \rangle. \quad (2)$$

In the large $t_1 - t_0$ and $t - t_1$ limit we have:

$$\begin{aligned}C_H(\vec{x}_2) &= \text{Lim}_{(t-t_1)\rightarrow\infty; (t_1-t_0)\rightarrow\infty} \tilde{C}_H(\vec{x}_2, t_1) \\ &= \sum_{\vec{p}, n} |\langle \Omega | J_H | H \rangle|^2 \frac{e^{-m_H(t-t_0)}}{4m_H^2} \langle H | j_0^u | n, \vec{p} \rangle \frac{e^{i\vec{p}\cdot\vec{x}_2}}{2E_n(\vec{p})} \langle n, \vec{p} | j_0^d | H \rangle.\end{aligned}\quad (3)$$

If we divide by the zero momentum hadron two-point function $G_H(\vec{0}, t-t_0)$ then the exponential dependence on $t-t_0$ and overlaps cancel and we obtain the expectation value of the two density insertions, $\langle H | j_0^u(\vec{x}_2) j_0^d | H \rangle$. In the non-relativistic limit, this expectation value gives the charge distribution of the hadron. It can be written in terms of the non-relativistic form factors [14]

$$\langle H | j_0^u(\vec{x}_2) j_0^d | H \rangle = \sum_{\vec{p}, n} F_{Hn}^u(\vec{p}) \frac{e^{i\vec{p}\cdot\vec{x}_2}}{2E_n(\vec{p})} F_{nH}^d(-\vec{p}) \quad (4)$$

where

$$F_{Hn}^u(\vec{p}) = \langle H | j_0^u | n, \vec{p} \rangle \quad (5)$$

The connected diagrams of the density-density correlators for mesons and baryons are shown in Fig. 1. We note here that the diagram depicted in Fig. 1 for baryons yields a correlator that depends only on one relative distance instead of two. To obtain, in the non-relativistic limit, the charge distribution that depends on the two relative distances one must calculate the three-density correlator. This requires the evaluation of two types of five-point functions shown in Fig. 2. In Ref. [16] the

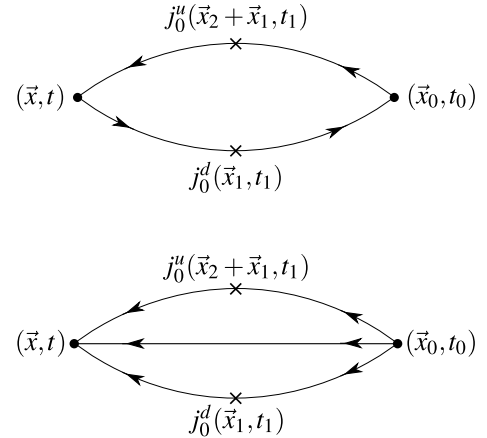


FIG. 1: Equal-time density-density correlators for mesons (upper diagram) and for baryons (lower diagram).

three-density correlator or five-point function was evaluated approximately for one of the diagrams shown in Fig. 2 for which each quark line has only one density insertion. It was shown that integrating over one relative

distance one obtains results that are consistent with the corresponding two-density correlator. For the work presented here we therefore only consider correlators with two-density insertions, which give the distribution of one quark relative to the other irrespective of the position of the third. In other words, in the non-relativistic limit, it corresponds to the one-body charge distribution.

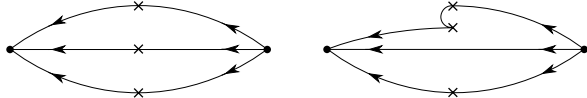


FIG. 2: The three density correlator for baryons.

What makes four-point functions harder to evaluate than three-point functions is the fact that we need to compute all-to-all propagators. Sequential inversions used in the evaluation of three-point functions can not be used here. The reason is that we are interested in obtaining the dependence in terms of a relative distance and therefore the spatial positions where the density operators are inserted involve the relative distance and can not be summed independently. Therefore the bulk of this work deals with the evaluation of the all-to-all propagators to sufficient accuracy.

III. STOCHASTIC TECHNIQUES

The technically challenging aspect of the calculation of the density-density correlators is the fact that the summation over sink and insertion coordinates requires knowledge of all-to-all propagators. A previous study has been carried out in the quenched approximation and using two dynamical degenerate Wilson fermions in which no summation was performed over the sink coordinates [16]. This eliminated the need of calculating all-to-all propagators at the cost of not explicitly projecting to zero momentum states, which instead were only obtained via the large Euclidean time suppression of higher momenta. In this work we use stochastic techniques to estimate the all-to-all propagators [26, 27] enabling us to sum over the sink coordinate and thus explicitly project to zero momentum initial and final states.

In order to evaluate the all-to-all propagator one begins by defining an ensemble of N_r noise vectors $\xi_\mu^a(\vec{x}, t)_r$ obeying to order $\left(\frac{1}{\sqrt{N_r}}\right)$

$$\langle \xi_\mu^a(\vec{x}, t) \rangle_r = 0 \quad \text{and} \\ \langle \xi_\mu^a(\vec{x}, t) \xi_{\mu'}^{a'}(\vec{x}', t') \rangle_r = \delta(\vec{x} - \vec{x}') \delta(t - t') \delta_{\mu\mu'} \delta_{aa'} \quad (6)$$

where μ and a are spinor and color indices respectively and r enumerates the vector in the stochastic ensemble. In particular, we use Z(2) noise where $\xi_\mu^a(\vec{x}, t) \in \{1, i, -1, -i\}$ with equal probability. By solving the Dirac equation with each of these N_r noise vectors as

the source, one obtains an ensemble of solution vectors:

$$\phi_\mu^a(x)_r = \sum_y G_{\mu\nu}^{ab}(x; y) \xi_\nu^b(y)_r \quad (7)$$

where ϕ is a solution vector and G is the inverse of the Dirac operator. If we now take the average over the product between solution and noise vectors over the stochastic ensemble, we obtain an estimate of the all-to-all propagator:

$$\langle \phi_\mu^a(x) \xi_\nu^{\dagger b}(y) \rangle_r = \sum_z G_{\mu\kappa}^{ac}(x; z) \langle \xi_\kappa^c(z) \xi_\nu^{\dagger b}(y) \rangle_r \\ = \sum_z G_{\mu\kappa}^{ac}(x; z) \delta(z - y) \delta_{\kappa\nu} \delta_{cb} \\ = G_{\mu\nu}^{ab}(x; y). \quad (8)$$

A well known technique used to suppress stochastic noise is dilution [28]. Within this technique, one distributes the elements of a noise vector over certain color, spin and volume components of multiple noise vectors setting the remaining components to zero. An example is spin dilution where the first noise vector has non zero entries only on the first spin component, the second vector only on the second spin component and so on. In this example, in order for the conditions in Eq. (6) to be satisfied, the total number of noise vectors N_r in the ensemble is restricted to multiplets of four. In Fig. 3 we show a schematic representation of n-fold dilution.

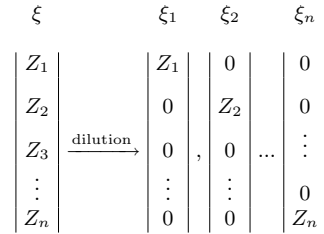


FIG. 3: A schematic representation of n-fold dilution. Z_i denotes a random complex number.

The more one dilutes, the closer an estimate one gains of the all-to-all propagator. This can be understood if one considers the extreme case where a noise vector is diluted over all color, spin and volume components. In this case one would have inverted for each color, spin and volume index thus obtaining the exact all-to-all propagator.

The straight forward way to carry out the computation of the density-density correlator is to expand Eq. (1) on the quark level and replace each all-to-all propagator with the stochastic average over the product between solution and noise vectors: $G_{\mu\nu}^{ab}(x; y) = \langle \phi_\mu^a(x) \xi_\nu^{\dagger b}(y) \rangle_r$. Throughout this paper we will refer to this as the direct method. As demonstrated in Section IV, a reasonable estimate of the all-to-all propagators can be computed through the direct method if a large enough number of stochastic inversions is carried out.

Significant improvement to the results obtained using the direct method is achieved by applying the so called

one-end trick. The one-end trick was originally devised to compute pion two-point functions [25]. In its original form it is based on the realization that by appropriately combining solution vectors one can derive the pion two-point function summed over both ends (source and sink). To be specific, let us consider the pion two-point function which, at the propagator level, is just the trace of the absolute square of the quark propagator:

$$\sum_{\vec{x}} \langle \pi(\vec{x}, t) | \pi(\vec{x}_0, t_0) \rangle = \sum_{\vec{x}} \text{Tr} [|G(\vec{x}, t; \vec{x}_0, t_0)|^2]. \quad (9)$$

Let us consider the stochastic average over the product between two solution vectors given by:

$$\sum_{\vec{x}} \langle \phi^*(\vec{x}, t; t_0) \phi(\vec{x}, t; t_0) \rangle_r, \quad (10)$$

where the t_0 appearing in the argument of the solution vector is to indicate that the noise vectors are localized on this time slice, i.e:

$$\xi_\mu^a(\vec{x}, t)_r = \xi_\mu^a(\vec{x}, t_0)_r \delta(t - t_0), \quad (11)$$

and hence

$$\phi_\mu^a(\vec{x}, t; t_0)_r = \sum_{\vec{y}} G_{\mu\nu}^{ab}(\vec{x}, t; \vec{y}, t_0) \xi_\nu^b(\vec{y}, t_0)_r. \quad (12)$$

By substituting for ϕ_μ^a in Eq. (10) we obtain:

$$\begin{aligned} & \sum_{\vec{x}} \langle \phi_\mu^{*a}(\vec{x}, t; t_0) \phi_\mu^a(\vec{x}, t; t_0) \rangle_r = \\ & \sum_{\vec{x}, \vec{x}'_0, \vec{x}''_0} G_{\mu\nu}^{*ab}(x; x'_0) G_{\mu\kappa}^{ac}(x; x''_0) \langle \xi_\nu^{*b}(x'_0) \xi_\kappa^c(x''_0) \rangle_r = \\ & \sum_{\vec{x}, \vec{x}'_0, \vec{x}''_0} G_{\mu\nu}^{*ab}(x; x'_0) G_{\mu\kappa}^{ac}(x; x''_0) \delta_{bc} \delta_{\nu\kappa} \delta(\vec{x}'_0 - \vec{x}''_0) = \\ & \sum_{\vec{x}, \vec{x}'_0} \text{Tr} [|G_{\mu\nu}^{ab}(x; x'_0)|^2] \end{aligned} \quad (13)$$

where $x'_0 = (t_0, \vec{x}'_0)$ and $x''_0 = (t_0, \vec{x}''_0)$. This is the pion two-point function given in Eq. (9) summed over all spatial source and sink coordinates. This double summation increases statistics by spatial volume as compared to the standard way where one computes two-point functions using a point-to-all propagator. The increase by spatial volume in statistics far outweighs the stochastic noise introduced by the stochastic inversion.

The pion two-point function is the simplest implementation of the one-end trick since the γ -structure of the interpolating fields combined with the backward propagator of the antiquark yield a simple trace over a product of two forward quark propagators. To apply the trick on an arbitrary meson two-point function with interpolating operators of the form $\bar{q}_f \Gamma q_{f'}$, where $f \neq f'$ label two flavors of quarks, not necessarily degenerate and Γ an arbitrary combination of gamma matrices, one

must use spin dilution. More explicitly, the noise vectors should be of the form $\xi_\mu^a(x)_{(r,\sigma)} = \xi^a(x)_r \delta_{\mu\sigma}$. The r index counts sets of noise vectors, each set containing four noise vectors carrying an index σ . We note here that this form of dilution is different than that described in the previous section. Here the Z(2) random numbers involved in the spin dilution are the same for each spin component entry. It can be easily confirmed that this choice satisfies the conditions in Eqs. (6); the sum over the stochastic ensemble now becomes a double sum (over r and σ) and $\langle \xi^a(x) \xi^{\dagger a'}(x') \rangle_r = \delta(x - x') \delta_{aa'}$. Within this notation the solution vectors are denoted as $\phi_\mu^a(x)_{(r,\sigma)} = \sum_{x_0} G_{\mu\nu}^{ab}(x; x_0) \xi^b(x_0)_r \delta_{\sigma\nu}$. Now one can appropriately combine the solution vectors to incorporate the Γ matrices involved and obtain the meson two-point function summed over both ends:

$$\begin{aligned} & \sum_{\vec{x}, r} \phi_\mu^a(\vec{x}, t; t_0)_{(r,\nu)} \Gamma'_{\nu\sigma} \phi_\kappa^{*a}(\vec{x}, t; t_0)_{(r,\sigma)} \bar{\Gamma}'_{\kappa\mu} = \\ & \sum_{\vec{x}, \vec{x}'_0, \vec{x}''_0} G_{\mu\nu}^{ab}(x; x'_0) \Gamma'_{\nu\sigma} G_{\kappa\sigma}^{*ab'}(x; x''_0) \bar{\Gamma}'_{\kappa\mu} \delta(\vec{x}'_0 - \vec{x}''_0) \delta_{bb'} = \\ & \sum_{\vec{x}, \vec{x}'_0} \text{Tr} [G(x; x_0) \Gamma G(x_0; x) \bar{\Gamma}] \end{aligned} \quad (14)$$

where $\Gamma' = \Gamma \gamma_5$ and $\bar{\Gamma} = \gamma_0 \Gamma^\dagger \gamma_0$. Thus the one-end trick can be generalized to an arbitrary meson interpolating field. We would like to note here that the automatic summation over the source using the same set of solution vectors selects a given momentum. Therefore the one-end trick by construction computes only two-point functions at a specific momentum. In the examples given above this momentum was set to zero. To compute meson two-point functions at various momenta, one must invert for a new set of solution vectors having previously transformed the noise vectors with an appropriate phase. In other words, one needs a new set of stochastic inversions for each momentum vector.

The crucial point that makes the one-end trick applicable to the evaluation of density-density correlators is the fact that the initial and final states have zero momentum. To show how to implement the one-end trick we consider the density-density correlator for an arbitrary meson with an interpolating operator of the form $\bar{q}_f \Gamma q_{f'}$, where $f \neq f'$:

$$\begin{aligned} C(\vec{x}_2) = & \sum_{\vec{x}_1, \vec{x}} \text{Tr} [\gamma_5 \gamma_0 G(x_1; x_0) \bar{\Gamma}' G^\dagger(x_{2+1}; x_0) \times \\ & \gamma_5 \gamma_0 G(x_{2+1}; x) \Gamma' G^\dagger(x_1; x)] \end{aligned} \quad (15)$$

where $x_{2+1} = (t_1, \vec{x}_2 + \vec{x}_1)$, $x_0 = (t_0, \vec{x}_0)$, $x_1 = (t_1, \vec{x}_1)$, $x = (t, \vec{x})$ and $\Gamma' = \Gamma \gamma_5$. Let us define:

$$S_{\mu\nu}^{ab}(\Gamma; x; y; t_0) \equiv \sum_r \phi_\mu^a(x; t_0)_{(r,\sigma)} \Gamma_{\sigma\kappa} \phi_\nu^{*b}(y; t_0)_{(r,\kappa)} \quad (16)$$

where $x = (t_x, \vec{x})$ and $y = (t_y, \vec{y})$ and the t_0 appearing in the argument of $S_{\mu\nu}^{ab}$ is to indicate that the noise vectors are localized on time-slice t_0 . Summation over all

repeated indices is implied. Assuming that the noise vectors are spin diluted in the manner described previously, we obtain

$$\begin{aligned}
S_{\mu\nu}^{ab}(\Gamma; x; y; t_0) &= \\
\sum_{\vec{x}_0, \vec{y}_0} G_{\mu\sigma}^{aa'}(\vec{x}, t_x; \vec{x}_0, t_0) \Gamma_{\sigma\kappa} G_{\nu\kappa}^{*bb'}(\vec{y}, t_y; \vec{y}_0, t_0) \delta_{a'b'} \delta(\vec{x}_0 - \vec{y}_0) \\
&= \sum_{\vec{x}_0} G(\vec{x}, t_x; \vec{x}_0, t_0) \Gamma G^\dagger(\vec{y}, t_y; \vec{x}_0, t_0) \Big|_{\mu\nu}^{ab}. \quad (17)
\end{aligned}$$

Thus in terms of the propagator defined in Eq. (16), the expression

$$\sum_{\vec{x}_1} Tr [\gamma_5 \gamma_0 S(\vec{\Gamma}'; x_1; x_{2+1}; t_0) \gamma_5 \gamma_0 S(\Gamma'; x_{2+1}; x_1; t)] \quad (18)$$

yields the density-density correlator of Eq. (15) with an additional summation over the source coordinate \vec{x}_0 . This is the generalization of the one-end trick to meson four-point correlators. It is apparent that one needs two sets of stochastic inversions: one with the noise vectors localized on the source time-slice t_0 and one with the noise vectors localized on the sink time-slice t .

IV. INTERPOLATING FIELDS AND LATTICE PARAMETERS

For the pion and the ρ -meson we compute the density-density correlators using both the one-end trick and the direct method. For the nucleon and the Δ it is not as straight forward to apply the one-end trick. The quark line propagating without a density insertion complicates the generalization of the trick to baryons since the propagators to be replaced by noise vectors are odd in number and therefore unlike for mesons the noise vectors cannot be grouped in pairs to yield δ -functions after summation. Thus in this work for the nucleon and Δ density-density correlators we only present results using the direct method.

One of our main goals is to detect a possible asymmetry in the charge distributions of these particles. For this purpose we select interpolating operators so that they project to physical spin states. For the mesons we use interpolating operators of the form: $J^M = \bar{u}\Gamma d$ with $\Gamma = \gamma_5$ for the case of the pion and $\Gamma = \{ \frac{\gamma_1 - i\gamma_2}{2}, \gamma_3, \frac{\gamma_1 + i\gamma_2}{2} \}$ for the +1, 0 and -1 polarizations of the vector meson respectively, where we have taken the z axis along the spin axis. For the nucleon we use $J_\sigma^N = \epsilon^{abc} u_\sigma^a (u^{b\top} C \gamma_5 d^c)$ where $C = \gamma_0 \gamma_2$. For the case of the Δ we opt to probe the spin $\pm \frac{3}{2}$ components. Thus we use the interpolating operators:

$$\begin{aligned}
J_{+\frac{3}{2}}^\Delta &= \frac{1}{\sqrt{3}} \epsilon^{abc} [u_1^a (2u^{b\top} C \Gamma_+ d^c) + d_1^a (u^{b\top} C \Gamma_+ u^c)] \\
J_{-\frac{3}{2}}^\Delta &= \frac{1}{\sqrt{3}} \epsilon^{abc} [u_2^a (2u^{b\top} C \Gamma_- d^c) + d_2^a (u^{b\top} C \Gamma_- u^c)] \quad (19)
\end{aligned}$$

where $\Gamma_\pm = (\gamma_1 \mp i\gamma_2)/2$.

Given the large number of inversions needed to compute the density-density correlators and the available computer resources, using dynamical Wilson fermions that are fast to invert is the only option at our disposal. We use two dynamical degenerate flavors of Wilson fermions at three pion masses. The exact parameters of the ensembles used are listed in Table I.

TABLE I: The first column gives the number of configurations analyzed, the second the value of the hopping parameter, the third the pion mass in GeV, the fourth the ratio of the pion mass to the ρ mass, the fifth the nucleon mass in GeV and the last column the size of the lattice. The first two sets of configurations are from Ref. [29] while the third is from Ref. [30]. The lattice spacing is determined from the nucleon mass at the chiral limit.

$\beta = 5.6, a^{-1} = 2.56(10) \text{ GeV}$					
N_{conf}	κ	m_π (GeV)	m_π/m_ρ	M_N (GeV)	$L^3 \times T$
185	0.1575	0.691(8)	0.701(9)	1.485(18)	$24^3 \times 40$
150	0.1580	0.509(8)	0.566(12)	1.280(26)	$24^3 \times 40$
200	0.15825	0.384(8)	0.453(27)	1.083(18)	$24^3 \times 32$
	$\kappa_c = 0.1585$	0		0.938(33)	

To suppress excited state contributions we use Gaussian or Wuppertal smeared sources [31]. In addition we apply hypercubic (HYP) smearing [32] on the gauge links that enter the smearing function that builds the Gaussian smearing function. The parameters that enter the Gaussian smearing function are taken from Ref. [33] where they were determined by optimizing ground state dominance for the nucleon. In fact, in Ref. [33] it was demonstrated that one can damp excited state contributions to the nucleon two-point function as early as 0.3 fm from the source time slice. The parameters for the HYP smearing are taken from Ref. [32].

For the computation of the correlators we take the time-slice of the density insertions to be at mid-point of the time separation between sink and source. For the direct method we take the time separation between the sink and the source to be $t - t_0 = 10a$ or 0.77 fm. This is the minimum time separation that is needed for the suppression of excited states. For the one-end trick the separation between sink and source is set to $t - t_0 = 14a$. The reason for taking a larger time separation when using the one-end trick lies in the accuracy of the results that allows for a larger time separation with a good signal. This allows us to check that indeed excited state contributions are sufficiently suppressed by comparing results at the two sink-source time separations.

We first give the details of the computation in the case of the direct method. We require two sets of stochastic propagators per configuration, one with the noise vectors localized on the insertion time-slice and one with the noise vectors localized on the sink. We also compute a point-to-all propagator from the source time-slice to all lattice sites. The noise vectors are diluted in color, spin and even-odd spatial sites. Dilution in time is automatic

here since we invert with the noise vectors localized on a single time-slice. Thus each noise vector is diluted to twenty-four independent noise vectors requiring twenty-four times more inversions. The number of noise vectors used is determined through a tuning process. For this tuning the Δ -baryon correlator at the lightest pion mass is considered. By comparing the decrease of the relative statistical error when increasing on one hand statistics and on the other hand the number of noise vectors used, we determine the optimum number of stochastic vectors. For this tuning we use 50 configurations and compute the Δ -baryon correlator for three, six and nine such 24-fold diluted noise vectors. For $N_r=3, 6$ and 9 we find a relative statistical error of 50%, 20% and 16% respectively. The fact that by doubling the number of noise vectors from 3 to 6 the statistical error decreases by more than one half is an indication that $N_r=3$ is too small yielding large stochastic noise. On the other hand, increasing the number of noise vectors from 6 to 9 the relative error decreases by $\sqrt{6/9}$, which is what is expected from scaling. This indicates that at this point increasing N_r or the number of configurations is equivalent. We thus fix the number of noise vectors to six. Since we carry out two sets of stochastic inversions, one at the sink and one at the insertion time-slice, and since we use color, spin and even-odd dilution we need 288 stochastic inversions per configuration. This amounts to a total of 300 inversions per density-density correlator if we additionally consider the point-to-all propagating from the origin. To increase statistics for the two ensembles corresponding to the two lightest pion masses needed for the baryons, we calculate density-density correlators using the first and second half time interval of each configuration. Furthermore, for the lightest pion mass we improve statistics by using $N_r=9$ noise vectors for the correlators. Thus for $\kappa = 0.1580$ we carry out 600 inversions per configuration while for $\kappa = 0.15825$ 888 inversions per configuration.

For the case of the mesons we have additionally computed the charge distributions using the one-end trick. Therefore for the computation of the meson density-density correlators additional inversions are carried out since the dilution method is specific to the one-end trick. Like for the direct method, two sets of inversions are needed to extract the density-density correlator using the one-end trick: one set with the noise source set at the source time t_0 and one set with the noise source set at the sink time t . We use eight spin-diluted noise vectors amounting to 32 inversions at the source and 32 at the sink or a total of 64 per configuration.

V. RESULTS

A. Comparison between the direct method and the one-end trick

For the meson density-density correlators we can compare results obtained using the direct method with those

using the one-end trick. Given that the time separation between sink and source is larger in the latter case this also provides a check of ground state dominance.

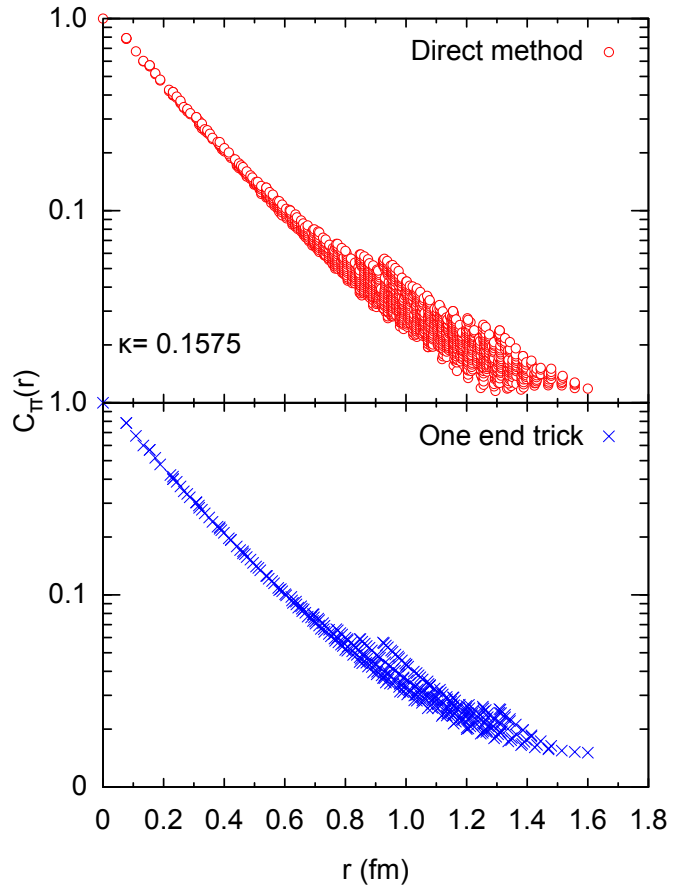


FIG. 4: The pion density-density correlator using the one-end trick (upper graph) and using the direct method (lower graph). The mean value of $C_\pi(r)$ is plotted as described in the text and error bars are suppressed for clarity.

The main source of error is due to the stochastic noise when computing the all-to-all propagators. By implementing the one-end trick, the four-point function is automatically summed over sink and source coordinates and thus this method is expected to suppress stochastic noise considerably.

In Fig. 4 we show the pion correlator computed using the one-end trick and the direct method as a function of the distance from the origin. To avoid having to display all lattice points in the graph we replace points lying within a cell of size $0.015 \text{ fm} \times 0.05$ by their average. We normalize the correlator by dividing by its value at the origin. The errors in Fig. 4 are not shown for clarity. As can be seen, we find that the two methods yield consistent results for the correlators. This demonstrates that excited states are sufficiently suppressed with a sink-source separation of 10 time slices. However, at a given distance r , the correlator computed using the direct method shows more spread than the one computed using the one-end trick. That this reflects larger statistical

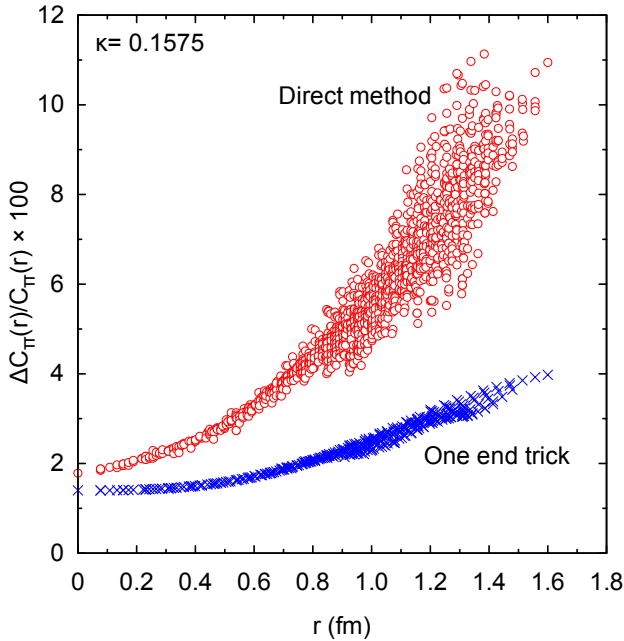


FIG. 5: Comparison between the relative error of the correlator computed with the one-end trick (blue crosses) and the direct method (red circles).

noise is shown in Fig. 5, where we compare the relative errors of the two binned correlators. As can be seen, at large distances the maximum relative error exhibited by the one-end trick method is around 4% while for the direct method exceeds 10%. This is a direct consequence of the double sum accomplished with the implementation of the one-end trick. In addition, when using the one-end trick the density-density correlator of a state of spin projection $m_z = 0$ is symmetric under reflections of the spatial coordinates i.e. $C(\vec{r}) = C(-\vec{r})$ by construction whereas in the direct method it is symmetric only statistically. For the $m_z = \pm 1$ projections of the vector meson we instead have $C^{m_z=+1}(\vec{r}) = C^{m_z=-1}(-\vec{r})$. Because of this symmetry we average over the results for the $m_z = +1$ and $m_z = -1$ spin projections and hereby denote this correlator by $m_z = \pm 1$. The same is done for the spin projections $m_z = \pm 3/2$ of the Δ . The reduction of the error by more than a factor two when using the one-end trick comes at a reduced computational cost. In the one-end trick the computation of the correlator is done using 64 inversions while for the direct method used in this comparison we carried out 300 inversions per configuration i.e. we need 4.7 times less inversions for twice the accuracy. This, combined with the fact that the computation using the one-end trick is carried out for a source-sink separation of 14 time slices while for the direct method we used a separation of 10 time slices and given that relative errors grow exponentially with the sink-source separation, clearly shows the superiority of the one-end trick.

One of the main goals of this calculation is to detect

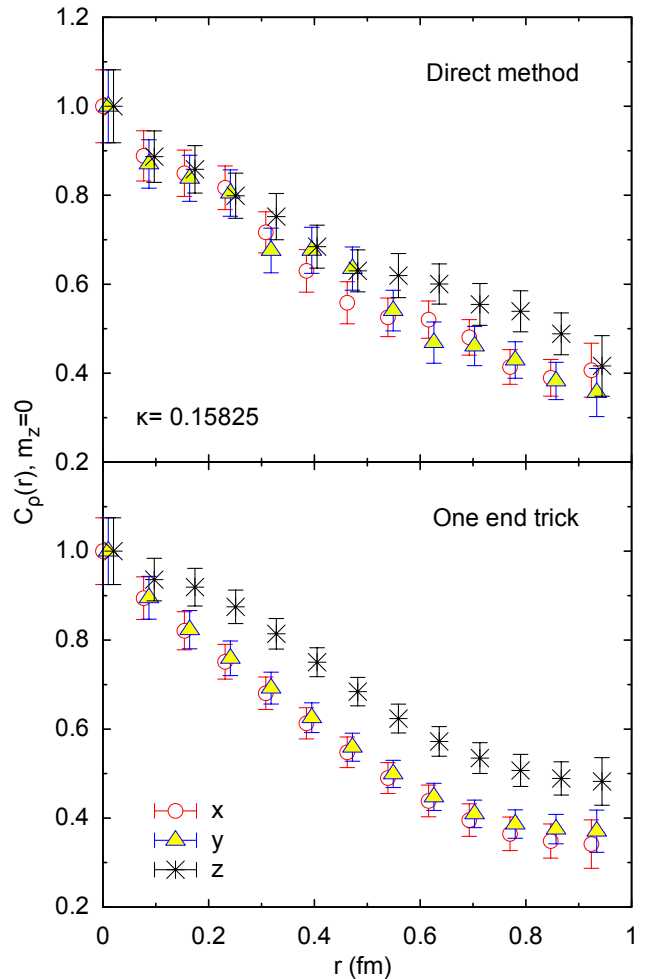


FIG. 6: Comparison between the vector meson $m_z = 0$ correlator projected along the three axes computed with the direct method (upper graph) and with the one-end trick (lower graph) using 200 configurations.

a possible asymmetry in the hadron charge distribution. In Fig. 6 we compare the two methods for the case of the $m_z = 0$ spin projection of the vector meson at the lowest pion mass available using the same number of configurations. Only the profile of the correlator along the three axes is plotted so that we can detect a possible asymmetry. As can be seen, an elongation along the z axis is clearly observed only when using the one-end trick. The statistical error in the direct method is not small enough to draw definite conclusions, since the projections of the correlator on the three axes are within error bars. Using the one-end trick the fluctuations are small enough to conclude that the vector meson is indeed prolonged along the z axis. When discussing results on baryon deformations one has to keep in mind that statistical fluctuations are larger than for mesons and that we can only apply the direct method making reaching conclusions for baryons more difficult.

Having demonstrated the effectiveness of the one-end

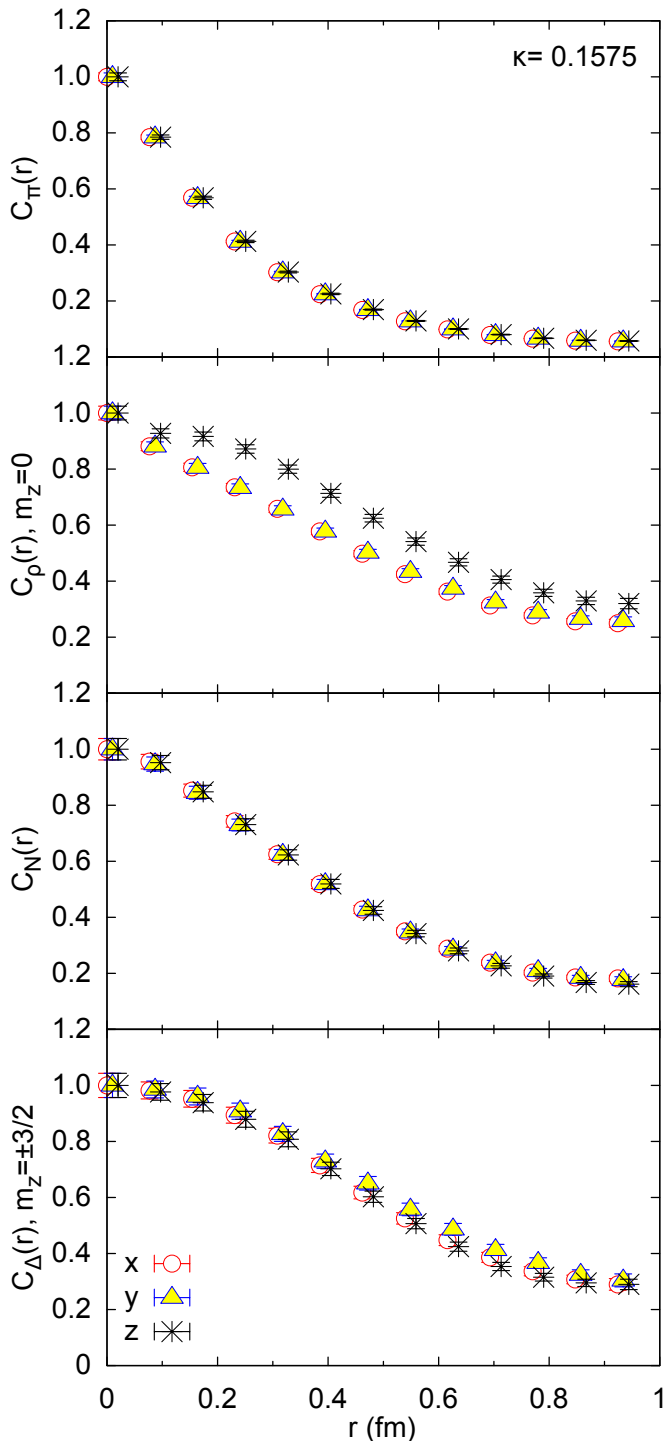


FIG. 7: Projections of the correlator along the three axes. From top to bottom: For the pion and the ρ - meson using the one-end trick with 64 inversions, for the nucleon and the Δ using the direct method with 300 inversion needed per configuration.

trick in suppressing stochastic noise, all meson observables that we present hereon are computed with the one-end trick.

B. Results without volume corrections

In Fig. 7 we show the density-density correlators for the pion and the spin zero projection ($m_z = 0$) of the ρ -meson using the one-end trick and for the nucleon and spin $m_z = \pm\frac{3}{2}$ projection of the Δ using the direct method. All correlators are projected along the three axes to display a possible asymmetry. This is done for the smallest pion mass available, namely $m_\pi = 0.691(8)$ GeV. As can be seen, a clear elongation of the vector meson along the z axis is observed confirming our previous results [16]. The asymmetry is clearly smaller than for the lightest pion mass shown in Fig. 6, showing that the deformation increases as the pion mass decreases. On the other hand, the nucleon shows no asymmetry within this method. For the Δ although there is a tendency for results projected along the z -axis to lie lower, all projections are well within error bars and therefore no asymmetry can be claimed. As pointed out when discussing results on the ρ using the direct method, statistical errors can hide possible deformation and one may have to improve on the errors to detect a small asymmetry.

Another way to visualize the asymmetry is to construct two-dimensional contour plots. Fig. 8 shows a contour plot of the $m_z = 0$ spin ρ -meson state on the $x - z$ plane. As can be seen, the contours are elongated along the z -axis as compare to a circle of radius equal to the distance along the x -axis for all three pion masses showing a clear asymmetry. This leads to the conclusion that the vector meson in the spin projection zero state is prolate. On the other hand, the $m_z = \pm 1$ ρ -meson state, shown in Fig. 9 shows the opposite behavior. Namely the correlator is found to be larger along the x -axis, as compared to a circle, evidence that in this spin state the ρ is in fact an oblate. This is in agreement with what is derived in Ref. [16] where it is shown that if the spin-0 state is a prolate the ± 1 channels will be oblate with about half the amount of deformation. The fact that the ρ -meson in its maximal spin projection state is an oblate is in agreement with a recent calculation of a negative electric quadrupole form factor evaluated in quenched lattice QCD [34].

C. Results after finite volume corrections

Density-density correlators computed in a finite box with periodic boundary conditions are susceptible to finite volume effects. Finite volume effects mostly affect the tail of the distributions and need to be corrected. To perform these corrections we follow the analysis developed in Ref. [14]. The density-density correlation function computed on a lattice of spatial dimension L can be written as an infinite sum over the Brillouin zones

$$C(\vec{r}) = \sum_{\vec{n}=0}^{\infty} C_0(\vec{r} + \vec{n}L) \quad (20)$$

where $C(\vec{r})$ is the density-density correlator computed on the periodic lattice and $C_0(\vec{r})$ is the “correct” correlator that one would compute if the lattice were of infinite size. Thus the correlation function computed in a finite box with periodic boundary conditions is in fact a sum of all images arising from the surrounding boxes. Since $C_0(\vec{r})$ is a fast decaying function, approximated by exponential or Gaussian dependence on the radius, it means that the leading contributions to the sum come from the nearest neighboring Brillouin zones. A two-dimensional sketch drawn in Fig. 10 demonstrates the images that contribute to the correlator. In this figure, the asterisk shows the origin of the fundamental cell (white box) while the triangles show the origins of the neighboring cells (gray boxes). To first order, the correlator computed in the white box is a superposition of the correlator with origin the asterisk and the eight correlators with origins the filled triangles, in accord with the expression given in Eq. (20). Thus the correlator that we compute on a peri-

odic lattice is overestimated. This is particularly severe close to the boundaries of the lattice where contributions from the images are largest. For example, the correlator at the distances indicated by the filled circles in Fig. 10 is approximately twice as large as the “correct” correlator since besides the contribution from the fundamental cell, a neighboring cell contributes equally as indicated by the dashed line. Similarly, the correlator computed at the distances indicated by the open circles at the corners of the fundamental cell is approximately four times larger since there are contributions from three neighboring cells, as shown by the dotted line.

This analysis can be extended to three dimensions. The correlator is twice as large at the six distances given by $\pm L/2\hat{n}_i$, $i = x, y, z$ where \hat{n}_i is the unit vector in the i -direction. Similarly, the correlator is four times as large at the twelve distances $L/2(\hat{n}_i \pm \hat{n}_j)$, $i \neq j$ and eight times as large at the eight corners $L/2(\pm\hat{n}_x \pm \hat{n}_y \pm \hat{n}_z)$.

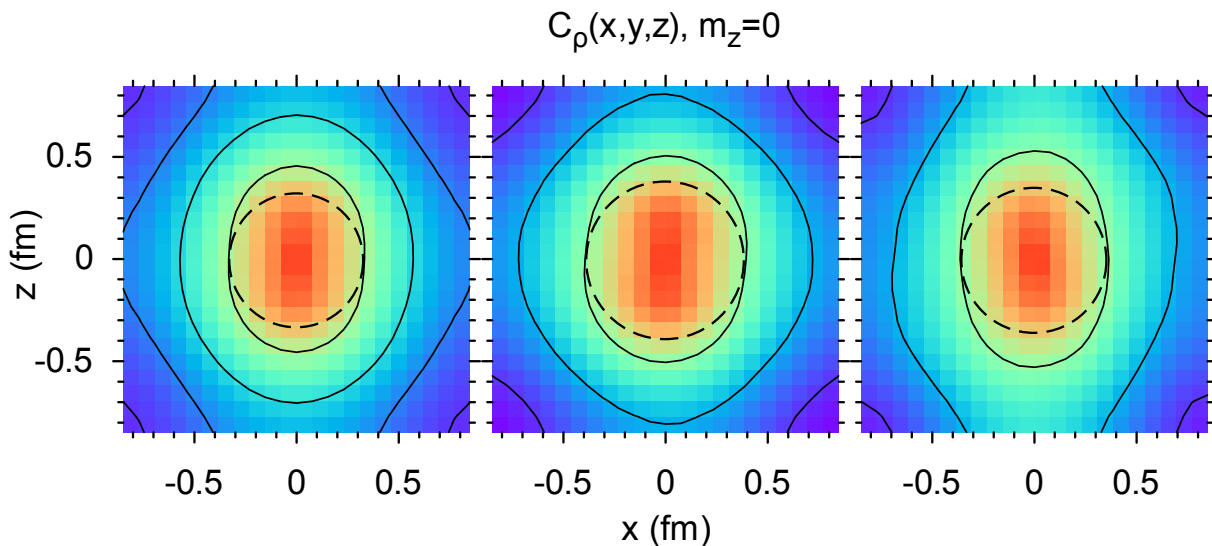


FIG. 8: The correlator of the ρ - meson, $m_z = 0$ projected on the $x - z$ plane for decreasing pion mass left to right. The dashed circles are to guide the eye.

All results that have been discussed so far are for the correlators computed on the lattice with no corrections applied for the images. For the analysis of quantities, such as the root mean squared radius, that are sensitive to the long distance behavior of the distributions it is important to take in to account the image contributions and define a corrected correlator. To correct for the images and extract $C_0(\vec{r})$ of Eq. (20) by knowing only $C(\vec{r})$ we need to have an Ansatz for the asymptotic behavior of $C_0(\vec{r})$. If the asymptotic behavior is known then we can subtract from the lattice data the contribution from the images, up to a given order, and extract $C_0(\vec{r})$. In this

work, we consider only nearest neighbor contributions to the correlator. Thus Eq. (20) becomes:

$$C(\vec{r}) \simeq \sum_{|\vec{n}| \in [0, \sqrt{3}]} C_0(\vec{r} + \vec{n}L). \quad (21)$$

We make an Ansatz for the functional form of $C_0(\vec{r})$ that provides a good description of the data. For instance for the pion correlator that is found to be independent of the angles, a spherically symmetric Ansatz is used. We then perform a least squares fit to the lattice data of the sum given on the right hand side of Eq. (21) extracting

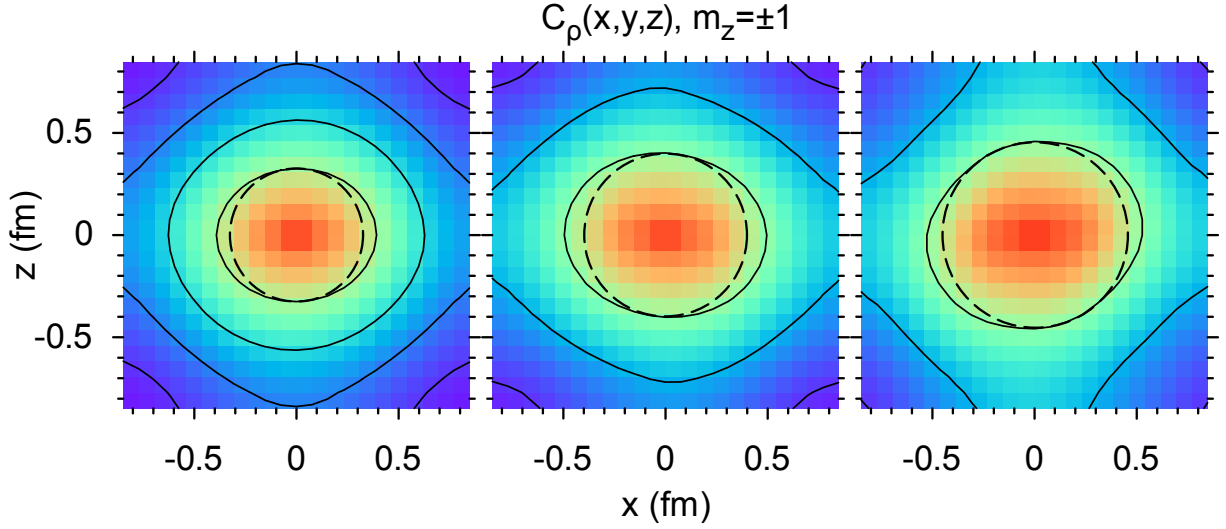


FIG. 9: The correlator of the ρ - meson, $m_z = \pm 1$ projected on the $x - z$ plane for decreasing pion mass left to right. The dashed circles are to guide the eye.

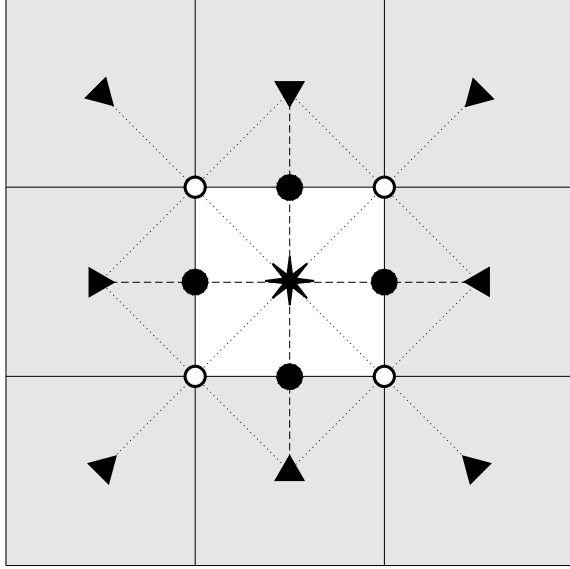


FIG. 10: Two-dimensional example of image contributions. The correlator computed at the filled circles (open circles) is approximately two (four) times larger than the “correct” correlator.

the fit parameters of the function that describes $C_0(\vec{r})$. The corrected correlator is then constructed by subtracting from the lattice data the images determined from the fitted function to obtain:

$$C^{\text{corr}}(\vec{r}) = C(\vec{r}) - \sum_{|\vec{n}| \in (0, \sqrt{3}]} C_0(\vec{r} + \vec{n}L). \quad (22)$$

The Ansätze for $C_0(\vec{r})$ for each particle are summarized below:

TABLE II: The parameters obtained from fitting the sum of images to the lattice data.

κ	0.1575	0.1580	0.15825
Mesons			
π			
A_0	0.986(21)	1.129(33)	1.437(78)
m_0	0.307(7)	0.405(11)	0.579(25)
σ	0.993(7)	0.884(9)	0.779(12)
$\rho, m_z = 0$			
A_0	0.969(13)	0.964(21)	0.919(31)
m_0	0.0173(19)	0.0140(26)	0.0093(26)
A_1	0.00170(31)	0.0031(16)	0.00183(46)
m_1	0.0466(87)	0.077(33)	0.0033(12)
σ	1.615(41)	1.646(69)	1.76(11)
$\rho, m_z = \pm 1$			
A_0	0.976(10)	0.961(16)	0.977(28)
m_0	0.0194(16)	0.0128(16)	0.0141(34)
A_1	-0.00113(18)	-0.00054(34)	-0.0012(17)
m_1	0.0560(91)	0.025(12)	0.066(69)
σ	1.577(30)	1.659(47)	1.613(87)
Baryons			
N			
A_0	1.014(39)	1.039(34)	1.057(34)
m_0	0.0673(40)	0.0698(44)	0.0548(38)
σ	1.451(20)	1.413(22)	1.450(24)
$\Delta, m_z = \pm \frac{3}{2}$			
A_0	1.024(22)	1.033(19)	1.023(16)
m_0	0.0125(11)	0.0130(12)	0.0087(8)
A_1	-0.00029(25)	-0.0007(14)	-0.00121(49)
m_1	0.024(13)	0.022(25)	0.077(30)
σ	1.750(32)	1.708(34)	1.787(33)

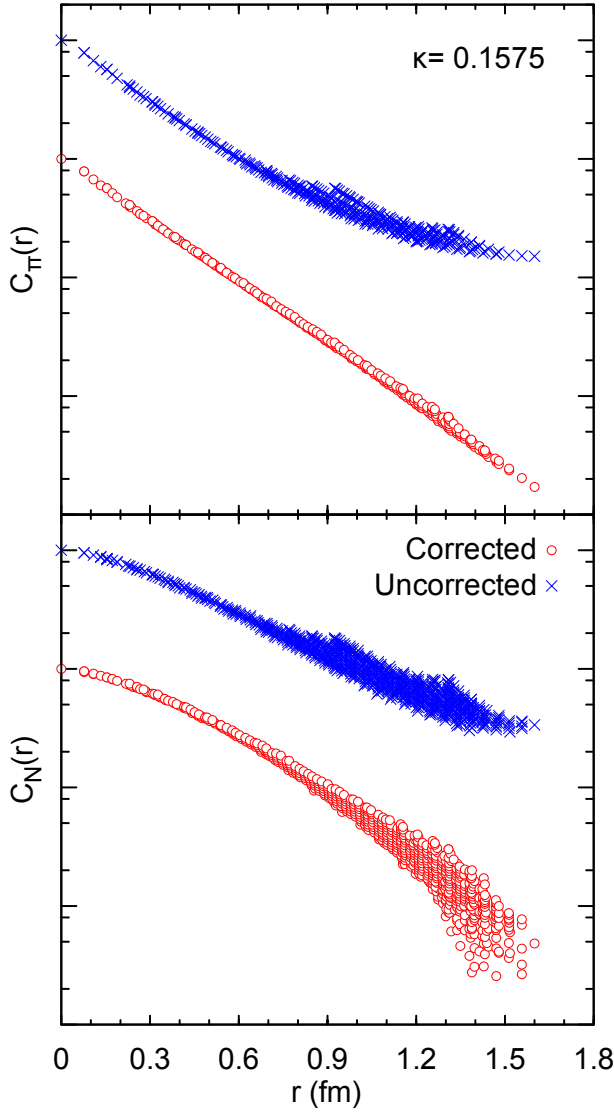


FIG. 11: The pion correlator (top) and the nucleon correlator (bottom) as computed on the lattice (crosses) and corrected for the images of nearest neighboring lattices (open circles). The corrected correlator is divided by a factor of ten for clarity. Data are binned and error bars are omitted to avoid cluttering.

$$\begin{aligned}
 C_0^\pi &= A_0 \exp(-m_0 r^\sigma), \\
 C_0^\rho &= \left[A_0 \exp(-m_0 r^\sigma) + A_1 \exp(-m_1 r^\sigma) r^2 P_2(\cos \theta) \right]^2, \\
 C_0^N &= \text{same as for } \pi, \\
 C_0^\Delta &= \text{same as for } \rho.
 \end{aligned} \tag{23}$$

As can be seen, for the pion and the nucleon we take spherical functions. For the case of the ρ we have parametrized the correlator in such a way so that an asymmetry, as seen in the uncorrected data, is allowed. For the Δ , although no asymmetry can be seen within

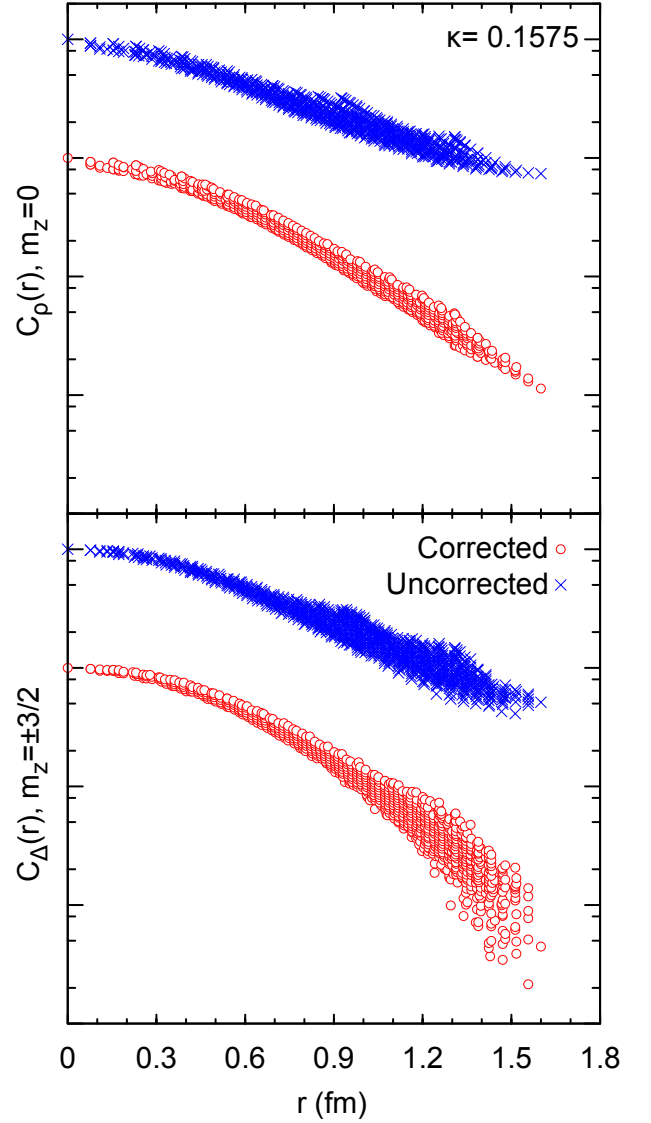


FIG. 12: The ρ -meson, $m_z = 0$ correlator (top) and the Δ , $m_z = \pm 3/2$ correlator (bottom). The notation is the same as that of Fig. 11.

our statistical errors we use the same Ansatz as for the ρ to see if the data allow for such a term.

Since the spatial part of the correlators is even under reflection, only $L = 0$ and $L = 2$ angular momentum quantum numbers are allowed. Thus for the ρ -meson and the Δ we include an $L = 2$ component by including the Legendre polynomial $P_2(\cos \theta)$. In Table II we summarize the fit parameters obtained. The fact that for the spin projection $m_z = 0$ ρ state the asymmetric term with coefficient A_1 is found non-zero and positive confirms that the correlator is indeed elongated along the z -axis (prolate) while the same parameter is consistently negative for the $m_z = \pm 1$ channels pointing to a correlator larger at the equator (oblate). For the Δ the A_1 coefficient comes out negative for all quark masses albeit with a large statistical error not allowing any definite

conclusions on the Δ shape.

In Figs. 11 and 12 we show a comparison between the raw lattice data and the lattice data after subtracting image contributions for the heaviest pion mass available. As can be seen, the correction procedure clearly compen-

sates for the images, i.e. the spikes at $L/2$, $\sqrt{2}L/2$ and $\sqrt{3}L/2$ are corrected for, leading to a smoother correlator that decreases more rapidly at the tails.

TABLE III: $\langle x^2 + y^2 \rangle/2$, $\langle z^2 \rangle$ and their difference for each particle at all three pion masses in fm^2 , left for mesons and right for baryons. All errors are jack - knife errors.

m_π^2 (GeV^2)	$\langle x^2 + y^2 \rangle/2$	$\langle z^2 \rangle$	$\langle z^2 - (x^2 + y^2)/2 \rangle$	m_π^2 (GeV^2)	$\langle x^2 + y^2 \rangle/2$	$\langle z^2 \rangle$	$\langle z^2 - (x^2 + y^2)/2 \rangle$
π				N			
0.477	0.1449(6)	0.1460(7)	0.0011(8)	0.477	0.164(1)	0.159(1)	-0.006(2)
0.259	0.1542(7)	0.1531(9)	-0.0010(10)	0.259	0.170(1)	0.168(2)	-0.002(3)
0.147	0.1529(7)	0.1533(14)	0.0005(18)	0.147	0.181(1)	0.182(2)	0.0008(31)
$\rho, m_z = 0$				$\Delta, m_z = \pm \frac{3}{2}$			
0.477	0.174(2)	0.192(2)	0.018(3)	0.477	0.177(1)	0.172(1)	-0.005(2)
0.259	0.188(4)	0.196(6)	0.007(7)	0.259	0.182(1)	0.180(2)	-0.001(2)
0.147	0.190(5)	0.207(6)	0.016(7)	0.147	0.195(2)	0.198(3)	0.003(4)
$\rho, m_z = \pm 1$							
0.477	0.183(1)	0.173(2)	-0.009(2)				
0.259	0.199(2)	0.186(2)	-0.013(2)				
0.147	0.200(4)	0.193(5)	-0.007(6)				

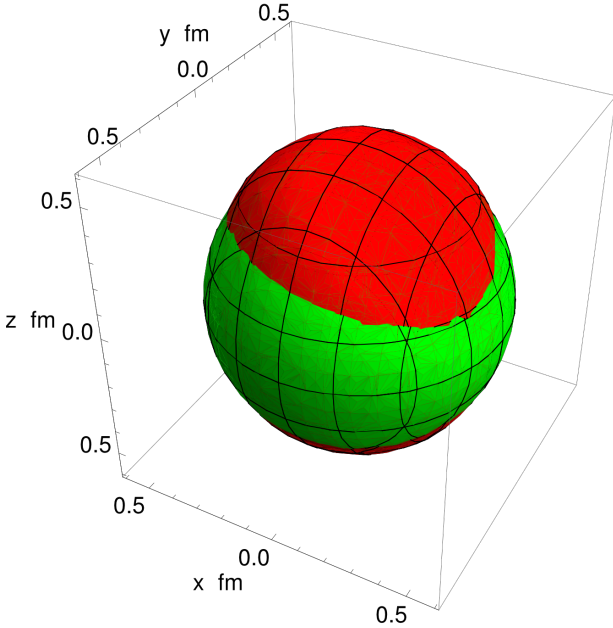


FIG. 13: Three-dimensional contour plot of the ρ -meson, $m_z = 0$ correlator (red or darker surface) compared to a sphere (green or lighter surface). The sphere radius is approximately 0.5 fm. The contour shows all \vec{r} such that $C(\vec{r}) = \frac{1}{2}C(0)$.

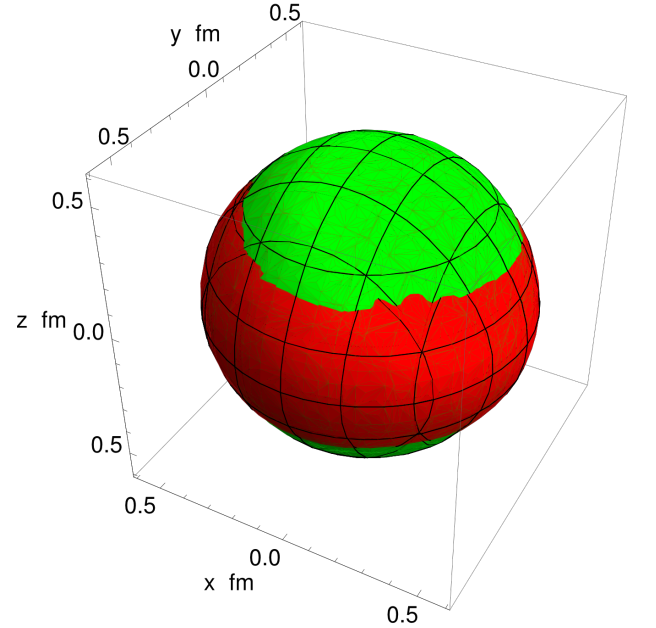


FIG. 14: Three-dimensional contour plot of the ρ -meson, $m_z = \pm 1$ correlator (red or darker surface) compared to a sphere (green or lighter surface). The sphere radius is approximately 0.5 fm. The contour shows all \vec{r} such that $C(\vec{r}) = \frac{1}{2}C(0)$.

Having corrected the data for the nearest images we can now proceed to a quantitative analysis of the particle charge distributions. In Table III we give $\langle x^2 + y^2 \rangle/2$,

$\langle z^2 \rangle$ and their difference for each particle at each pion mass available. All errors are jack - knife errors. Here, the moments presented are computed using the corrected

correlator:

$$\langle \mathcal{O} \rangle = \frac{\sum_{\vec{r}} \mathcal{O}(\vec{r}) C^{\text{corr}}(\vec{r})}{\sum_{\vec{r}} C^{\text{corr}}(\vec{r})}. \quad (24)$$

From the difference $\langle z^2 - \frac{x^2+y^2}{2} \rangle$ we see once again that the $m_z = 0$ projection of the ρ is larger along the z axis while the $m_z = \pm 1$ projections are larger along the equator. An additional observation here is that the asymmetry of the $m_z = \pm 1$ projections is approximately half that of the $m_z = 0$ projection, thus verifying the result reached in Ref.[16]. For the case of the Δ on the other hand a spherical distribution cannot be excluded, although for the two lightest pion masses we increase the statistics by computing the correlators using the first and the second half temporal extent of the lattice and by using $N_r=9$ noise vectors for the smallest of the two values.

The asymmetry in the ρ is nicely represented by a three-dimensional contour plot. In Figs. 13 and 14 we show contour surfaces for the ρ -meson in the $m_z = 0$ and $m_z = \pm 1$ channels respectively, at the intermediate pion mass. The correlator is compared to a sphere centered at the origin. Once again we see that the $m_z = 0$ state is elongated along the poles while the $m_z = \pm 1$ channels are flatter.

VI. SUMMARY AND CONCLUSIONS

In this work we develop the formalism for the exact evaluation of the equal time density-density correlators, which in the non-relativistic limit reduce to the hadron charge distribution. The pion, ρ -meson, nucleon and Δ density-density correlators are evaluated using dynamical Wilson fermions down to a pion mass of 384 MeV. The all-to-all propagators needed for the calculation of these correlators are computed using stochastic techniques combined with dilution. Having the all-to-all propagators is required so that an explicit projection to

zero momentum initial and final states is carried out. In the meson-sector we implemented the one-end trick, which leads to a significant improvement in the accuracy with which the density-density correlators are obtained. This improved accuracy is needed to conclude with certainty that the ρ -meson is deformed. The ρ is found to be a prolate when in the spin projection zero state and an oblate in the spin projection ± 1 state. This result corroborates previous studies where the density-density correlator of the ρ was calculated without explicit zero-momentum projection and with less accuracy [16]. It is also in agreement with a negative quadrupole form factor calculated recently on the lattice [34]. For the baryons a spherical distribution can not be excluded given the present statistical errors despite increase in statistics.

Finite spatial volume effects affect mainly the long distance behavior of the correlators. By adopting an Ansatz for the asymptotic dependence of the correlators we correct for these finite volume effects by subtracting the first image contributions. The functional form determined from fits to the corrected data confirm a deformed shape for the ρ meson. For the Δ , although the fits allow for a small deformation, the statistical error is too large to exclude a spherical distribution. Further improvements in the evaluation of all-to-all propagators such as combination of stochastic techniques and lower eigenmode projection are currently being investigated by a number of groups with promising results [35] that have potential application in the study of baryon density-density correlators.

Acknowledgments

G. K. would like to acknowledge support by the Cyprus Research Promotion Foundation. The computations for this work were partly carried out on the IBM Power6 575 machine at NIC, Jülich, Germany.

-
- [1] A. Bohr and B. R. Mottelson, *Nuclear Structure Vol. II: Nuclear Deformations* (Benjamin, New York, 1975).
 - [2] . Y. Lee et al., Phys. Rev. **C12**, 1483 (1975).
 - [3] R. S. Berry, *The lesson of Qunatum Theory* (North-Holland, 1986).
 - [4] S. C. Ceraulo and R. S. Berry, Phys. Rev. **A44**, 4145 (1991).
 - [5] G. Blanpied et al. (LEGS), Phys. Rev. Lett. **76**, 1023 (1996).
 - [6] T. Pospischil et al., Phys. Rev. Lett. **86**, 2959 (2001).
 - [7] C. Mertz et al., Phys. Rev. Lett. **86**, 2963 (2001), nucl-ex/9902012.
 - [8] K. Joo et al. (CLAS), Phys. Rev. Lett. **88**, 122001 (2002), hep-ex/0110007.
 - [9] C. N. Papanicolas, Eur. Phys. J. **A18**, 141 (2003).
 - [10] C. N. Papanicolas and A. M. Bernstein, AIP Conference Proceedings **104**, 1 (2007).
 - [11] C. Alexandrou et al., Phys. Rev. **D77**, 085012 (2008), 0710.4621.
 - [12] C. Alexandrou, Nucl. Phys. Proc. Suppl. **128**, 1 (2004), nucl-th/0311007.
 - [13] C. Alexandrou, AIP Conf.Proc. **904**, 1 (2007), hep-lat/0608007.
 - [14] M. Burkardt, J. M. Grandy, and J. W. Negele, Ann. Phys. **238**, 441 (1995), hep-lat/9406009.
 - [15] R. Gupta, D. Daniel, and J. Grandy, Nucl. Phys. Proc. Suppl. **30**, 419 (1993), hep-lat/9211057.
 - [16] C. Alexandrou, P. de Forcrand, and A. Tsapalis, Phys. Rev. **D66**, 094503 (2002), hep-lat/0206026.
 - [17] C. Alexandrou, P. de Forcrand, and A. Tsapalis, Nucl. Phys. Proc. Suppl. **119**, 422 (2003), hep-lat/0209067.
 - [18] C. Alexandrou, P. de Forcrand, and A. Tsapalis, Nucl.

- Phys. **A721**, 907 (2003), nucl-th/0212005.
- [19] C. Alexandrou, P. de Forcrand, and A. Tsapalis, Phys. Rev. **D68**, 074504 (2003), hep-lat/0307009.
- [20] C. Alexandrou, P. de Forcrand, and A. Tsapalis, Nucl. Phys. Proc. Suppl. **129**, 221 (2004), hep-lat/0309064.
- [21] C. Alexandrou, G. Koutsou, and A. Tsapalis, Nucl. Phys. Proc. Suppl. **140**, 275 (2005), hep-lat/0409065.
- [22] C. Alexandrou, P. Dimopoulos, G. Koutsou, and H. Neff, PoS **LAT2005**, 030 (2006), hep-lat/0509125.
- [23] C. Alexandrou, G. Koutsou, and H. Neff, PoS **LAT2006**, 113 (2006), hep-lat/0610039.
- [24] C. Alexandrou and G. Koutsou, PoS **LAT2007**, 150 (2007), 0710.2441.
- [25] C. McNeile and C. Michael (UKQCD), Phys. Rev. **D73**, 074506 (2006), hep-lat/0603007.
- [26] C. Michael and J. Peisa (UKQCD), Phys. Rev. **D58**, 034506 (1998), hep-lat/9802015.
- [27] S. Collins, G. Bali, and A. Schafer, PoS **LAT2007**, 141 (2007), 0709.3217.
- [28] J. Foley et al., Comput. Phys. Commun. **172**, 145 (2005), hep-lat/0505023.
- [29] B. Orth, T. Lippert, and K. Schilling, Phys. Rev. **D72**, 014503 (2005), hep-lat/0503016.
- [30] K. Jansen, A. Shindler, C. Urbach, and U. Wenger, PoS **LAT2005**, 118 (2006), hep-lat/0510064.
- [31] C. Alexandrou, S. Gusken, F. Jegerlehner, K. Schilling, and R. Sommer, Nucl. Phys. **B414**, 815 (1994), hep-lat/9211042.
- [32] A. Hasenfratz and F. Knechtli, Phys. Rev. **D64**, 034504 (2001), hep-lat/0103029.
- [33] C. Alexandrou, G. Koutsou, J. W. Negele, and A. Tsapalis, Phys. Rev. **D74**, 034508 (2006), hep-lat/0605017.
- [34] J. N. Hedditch et al., Phys. Rev. **D75**, 094504 (2007), hep-lat/0703014.
- [35] C. Morningstar, PoS **LAT2008**, 00 (2008).